Q. J. R. Meteorol. Soc. (2000), **126**, pp. 2175–2198

Atmospheric response to sea surface temperature anomalies during El Niño 1997/98 as simulated by ECHAM4

By ANSELM GRÖTZNER*, MOJIB LATIF and DIETMAR DOMMENGET
Max-Planck-Institut für Meteorologie, Germany

(Received 22 January 1999; revised 11 April 2000)

SUMMARY

One of the strongest El-Niño events on record was observed in 1997/98, a time period characterized by many strong climate anomalies all over the globe. To study the origin of these climate anomalies, ensemble experiments have been performed with the ECHAM4 atmospheric general circulation model at T42 resolution forced by observed sea surface temperatures (SSTs). Many of the observed climate anomalies and the well known El Niño Southern Oscillation teleconnection patterns could be reproduced by the ensemble integrations. In particular, the model reproduces the observed weakening of the trade winds, although it fails to simulate the early decline of the Southern Oscillation Index in November 1997. The observed climate anomalies over the Pacific, the Americas, and the Atlantic were successfully simulated. The model also reproduces the observed splitting of the jet over the North Atlantic which caused a very mild winter in western Europe. Our results do not indicate that the intense 1997 summer rainfalls leading to severe flooding in eastern central Europe were related to El Niño. With respect to the Indian Ocean, India, Australia, and southern Africa, the results were less satisfying. For example, the model yields reduced Indian monsoon rainfall which has not been observed. Additional experiments with SST anomalies restricted to particular ocean basins reveal that most of the atmospheric climate anomalies in 1997/98 were related to SST anomalies in the tropical Pacific. In particular, Atlantic SST anomalies had only a marginal impact on the atmosphere.

KEYWORDS: Climate modelling ENSO General circulation model Teleconnections

1. INTRODUCTION

After a relatively long period of moderate variability in tropical Pacific sea surface temperatures (SSTs), an extraordinarily strong El Niño occurred in 1997/98. Its strength was comparable to that of the 1982/83 event, the strongest observed so far. The development of tropical Pacific SST anomalies in 1997/98 was successfully predicted by several coupled ocean–atmosphere general circulation models (AGCMs; e.g. Stockdale *et al.* 1998). During this time not only the tropical Pacific region but also many other areas all over the globe experienced strong climate anomalies. It is well known that equatorial Pacific SST anomalies (SSTAs) affect not only the tropical Pacific atmosphere but also many other regions all over the globe (e.g. Halpert and Ropolewski 1992), since the anomalous diabatic heating of the atmosphere related to El Niño induces global circulation changes. Many of the climate anomalies observed during 1997/98 fit into the canonical picture derived from previous El Niños. Marked deviations, however, were also observed. For example, no strong precipitation anomalies occurred across the Indian subcontinent during northern hemispheric summer, although the monsoonal circulation in the upper troposphere was anomalously weak. Likewise, drier than normal conditions in north-eastern Australia, as expected from previous El Niños, were absent during winter 1997/98. Such differences in the response patterns can arise from specific features of the individual El Niños, namely: the structure of the equatorial heat source; the type of interaction of the propagating Rossby waves with the extratropical background mean flow; and the chaotic nature of mid-latitude weather systems (a review is given in Trenberth *et al.* 1998). Compared with previous

* Corresponding author: Max-Planck-Institut für Meteorologie, Bunderstrasse 55, D-20146 Hamburg, Germany.

El Niños, the 1997/98 event attained large amplitudes as early as June, which might have modified the summer response. Analyses of observed data can give only limited insight into such details, since the estimate of the SST-forced signal is usually based on composite analyses. Such procedures highlight the common features but ignore the differences between events. This could be overcome with a long enough observational record; at present, however, it is too short.

The systematic response of the atmosphere to SSTAs is always embedded in the internal variability of the atmosphere, which arises from the chaotic nature of atmospheric weather. The task is to separate the SST-forced signal from the internally generated noise. It is difficult to derive such a separation of signal and noise using observations, since they represent only a single realization of the random noise. An alternative is to use AGCMs. Ensemble experiments with common SST forcing, but different realizations of atmospheric weather, have to be considered. The ensemble mean can be viewed as an expression of the externally forced signal, while the spread of the individual realizations gives a measure of the internally generated noise. The signal-to-noise ratio provides information about the predictability, at least within the model environment. In a variety of modelling studies related to previous El Niño Southern Oscillation (ENSO) extremes, such separations of signal and noise have been performed and the global links to tropical Pacific SSTAs investigated. The SST-forced component of atmospheric variability is clearly dominant in the tropics, while the extratropics generally exhibit only a rather small signal-to-noise ratio (Dix and Hunt 1995; Harzallah and Sardourny 1995; Kumar and Hoerling 1995; Stern and Miyakoda 1995; Smith 1995). However, at least in the North Pacific and North American regions, the forced component of atmospheric variability is strong enough to make probabilistic climate forecasts for those extratropical areas feasible, especially in winter and spring (Rowell 1998). The main source of forced atmospheric variability, both in the tropics and extratropics, must be attributed to the tropical Pacific, although the other tropical oceans seem to be influential on a regional scale (Rowell *et al.* 1995; Moron *et al.* 1995; Yang *et al.* 1995). The role of extratropical SSTAs in forcing the atmosphere is still a matter of debate (e.g. Trenberth *et al.* 1998), but their influence seems to be small on interannual time-scales. The same seems to be the case for the land surfaces (Zwiers 1996). The impact of tropical Pacific forcing is especially large when the ENSO is strong (Branković and Palmer 1997; Barnett 1997; Hoerling and Kumar 1997), implying much better reproducibility and predictability of climate anomalies in such years. However, the performance of the AGCMs is still far from perfect (e.g. Kumar *et al.* 1996) and their skill does not exceed that of statistical prediction methods (Anderson *et al.* 1999). Nevertheless, the potential of such models in predicting ENSO-related climate anomalies has already been shown in the two-tiered approach (Bengtsson *et al.* 1993), where SSTAs predicted by a relatively simple regional model are used to force an ensemble of AGCM integrations. Such a procedure allows for useful climate forecasts some seasons ahead, at least for strong ENSO events (Barnett *et al.* 1994).

We have performed ensemble integrations with the AGCM ECHAM4, which may help to clarify which of the observed global climate anomalies in 1997/98 were ENSO-related and which were caused by non ENSO-related SSTAs or internal variability. Our paper is organized as follows. We describe the experimental design in section 2. In section 3 we present the overall performance of the ECHAM4 model in simulating ENSO teleconnections. The atmospheric response to global 1997/98 SSTAs is discussed in section 4. Additional sensitivity experiments prescribing SSTAs in individual ocean basins are described in section 5. The paper concludes with a summary of our major findings in section 6.

2. THE EXPERIMENTS

The ECHAM4 AGCM has a spectral resolution of T42 (~2.8°) and 19 levels in the vertical, and contains all physical parametrizations required for climate simulations (Roeckner *et al.* 1996a). This model has also been run in coupled mode using different ocean components in climate variability studies (e.g. Roeckner *et al.* 1996b; Frey *et al.* 1997) and experimental El Niño forecasts (Oberhuber *et al.* 1998). Three types of ensemble experiments have been conducted for the 1997/98 El Niño event. In the first ensemble the model was forced by global observed SSTs (Reynolds and Smith 1994) for the period January 1997 to February 1998. Figure 1 displays these SSTAs for June, July and August (JJA) 1997 and December, January and February (DJF) 1997/98. Unlike previous El Niños, the tropical eastern Pacific already exhibited strong positive temperature anomalies of more than 3 degC in JJA 1997. Increasing only moderately in amplitude, the anomalies spread westward, covering a larger area by the end of the year. However, other regions of the globe were also covered by anomalous SSTs. Positive temperature anomalies were observed in the Gulf of Alaska and along the North American Pacific coast during JJA. During DJF 1997/98 higher than normal temperatures occurred in the tropical Atlantic and Indian Oceans, and along the eastern coasts of Asia and Australia, while both the subtropical South Pacific and mid-latitude North Pacific were colder than normal. Many of these SSTAs fit into the canonical ENSO picture (e.g. Latif *et al.* 1997; Wallace *et al.* 1998). However, positive SSTAs east of Australia are not typical of El Niño years. The anomalies in the Indian Ocean were much higher than usual and were probably related to processes within the Indian Ocean itself (Webster *et al.* 1999). Moreover, strong SSTAs were also observed in the North Atlantic. They attained maximum values of more than +2 degC along the North African coast and −3 degC in the Labrador Sea in DJF 1997/98. These anomalies were present throughout 1997; their source, however, remains unclear. In order to assess the impact of regional SSTAs we carried out additional ensemble experiments. A second ensemble was performed prescribeding only Pacific SSTAs north of 30°S, and a third ensemble experiment was conducted using Atlantic SSTAs north of the equator. The last two ensembles were restricted to DJF 1997/98.

Since the atmosphere is characterized by a large amount of unpredictable noise, the experiments have been carried out using ensembles. Ten members were used in each ensemble experiment, each ensemble member being characterized by a different realization of atmospheric weather. The ensemble-mean response can be regarded as the SST-forced signal, while the scatter within the ensemble provides a measure of the uncertainty. The years 1979–94 were chosen as a reference period and a 26-year control experiment with climatological SSTs derived from this period was performed. One should keep in mind that the years 1979–1994 were characterized by quite high temperatures, therefore anomalies shown here may appear weaker compared with other climatologies. Departures of the ensemble statistics from those of the control run, to be regarded as the forced SST signal, were tested for statistical significance by applying a nonparametric Wilcoxon–Mann–Whitney U-test (Siegel 1996). In contrast with a t test this takes into account the full probability distribution, and does not rely on any assumption regarding the shape of the distribution. This is especially advantageous in regard to precipitation which is generally non-normally distributed.

Re-analyses provided by the National Centers for Environmental Prediction (NCEP) were chosen to verify mean-sea-level pressure (m.s.l.p.) and 850 hPa temperature ($T_{850\text{hPa}}$) anomalies, and anomaly fields were generated with respect to the same 1979–94 reference period. Observations of global precipitation (P) anomaly fields are

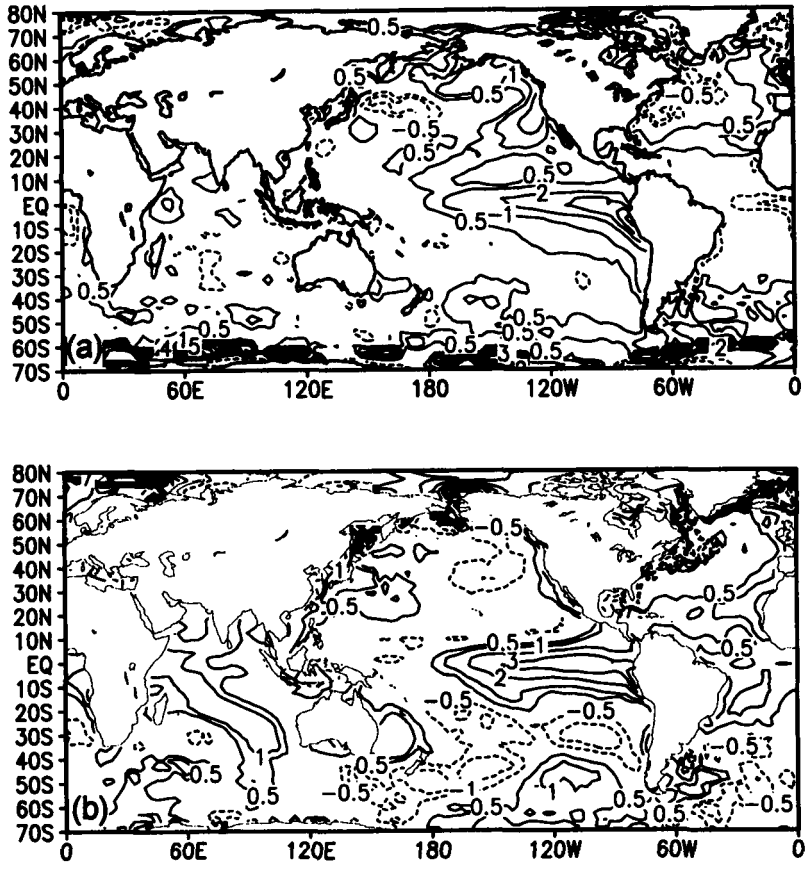

Figure 1. Observed sea surface temperature (SST) anomalies (degC) for: (a) June to August 1997, and (b) December to February 1997/98. The years 1979 to 1994 were chosen as the reference period. Contour lines are shown for ±0.5, 1, 2, 3, 4, 5.

obtained from the CAMS/OPI* (Xie and Arkin 1997) dataset provided by the NOAA† Climate Prediction Centre (CPC). These data consist of a blend of land-based rain-gauge measurements and satellite retrievals over the oceans; they are available almost in real time but their accuracy is limited, therefore they should only be considered qualitatively useful.

From a single event such as the 1997/98 El Niño it is difficult to decide whether discrepancies between observed and simulated climate anomalies are related to systematic model deficiencies or to atmospheric noise. For the model, the impact of atmospheric noise can be handled by applying the ensemble technique. However, the observed anomalies represent only a single realization and thus contain both the effects of anomalous SST forcing and random internal variability. On the other hand, the simulated effects of SSTAs might be compromised by model errors. To assess the overall performance of the ECHAM4 model in simulating ENSO teleconnections, additional long-term experiments forced by historical SSTs have been conducted. Four experiments forced by the GISST2.2‡ dataset (Rayner *et al.* 1996) for the period 1951–94

* CAMS: Climate Anomaly Monitoring System. OPI: OLR (outgoing long-wave radiation) Precipitation Index.
† National Oceanic and Atmospheric Administration.
‡ GISST: Global Ice and SST.

were conducted, which differed only in their initial conditions. The simulated anomalies for m.s.l.p. and T_{850hPa} were compared with the NCEP re-analyses. For precipitation we have chosen a dataset provided by Hulme (1991). This dataset only contains rain-gauge measurements over land; however, it covers the full period 1951–94, and therefore allows for more reliable statistics than the relatively short CAMS/OPI dataset. From such comparisons it is possible to determine those regions where the model simulations are skilful. Applied to the 1997/98 event, such 'skill masks' help to distinguish where discrepancies between forecasts and observations result from model deficiencies, and where they may be related to atmospheric noise. Discrepancies between the model simulations and the observations in 1997/98 in regions where the model exhibits a reasonable hindcast skill are likely to be caused by internal variability. In regions where the model does not show any skill, such discrepancies are more likely to result from model deficiencies. If a typical ENSO teleconnection is missing from both model and data in 1997/98 and the model is not skilful in this region, the results should also be disregarded. However, when both model and observations show an unexpected signal for 1997/98, it is unlikely that this consistency occurs just by chance; rather, there is a high probability that it is related to the extraordinary strength of El Niño 1997/98.

3. Performance of the ECHAM4 model in simulating previous ENSO-related anomalies

The impact of SSTAs and the reproduction of ENSO teleconnections simulated by an AGCM can be shown by many different methods including composites, analysis of variance (ANOVA), and pattern correlations. Here, global correlation patterns of m.s.l.p., T_{850hPa} and P with the NINO3 area (90°–150°W, 5°S–5°N) SSTA time series from the ensemble forced by the GISST data are compared with those derived from the NCEP re-analyses and precipitation data. Since the re-analyses start in 1958, the correlation analysis for m.s.l.p. and T_{850hPa} is limited to 1958–94, while the precipitation data cover the time period of the experiments. Correlation patterns derived from an ensemble mean are not directly comparable to a single realization as given by the observations, since the averaging procedure smooths the noise and enhances the level of correlation. Therefore, the correlation patterns have been calculated for the individual realizations and averaged afterwards. Such a procedure highlights those regions in which all realizations agree with each other, which yields a more conservative estimate.

The simulated signature of the Southern Oscillation in JJA (Fig. 2(a)) with negative correlations over the eastern Pacific, and positive values over Indonesia, Australia and the Indian Ocean is in good agreement with the re-analyses (Fig. 2(c)). However, the observed link to the tropical Atlantic is missing in the model, and the simulated positive connection to south-east Asia is unrealistic. In DJF most of the observed m.s.l.p. anomaly pattern (Fig. 2(d)) can be reproduced by ECHAM4 (Fig. 2(b)). The model yields negative correlations over the eastern Pacific and positive values similar to those observed over the tropical Atlantic, Africa, the warm-pool region and in two tongues north and south of the eastern Pacific negative centre.

In DJF the observed Pacific–North America (PNA) pattern, with negative correlations over the north-western Pacific, the Bering Sea and the western Atlantic is also found in the model. However, the model's Walker cell reacts too strongly to SSTAs in the eastern Pacific, which is reflected in this analysis by much higher correlations compared with the re-analyses. For the same reason, excessive negative values are simulated over northern South America. On the other hand, the positive ENSO link to the Indian Ocean appears too weak in the simulations. A band of negative correlations extending from

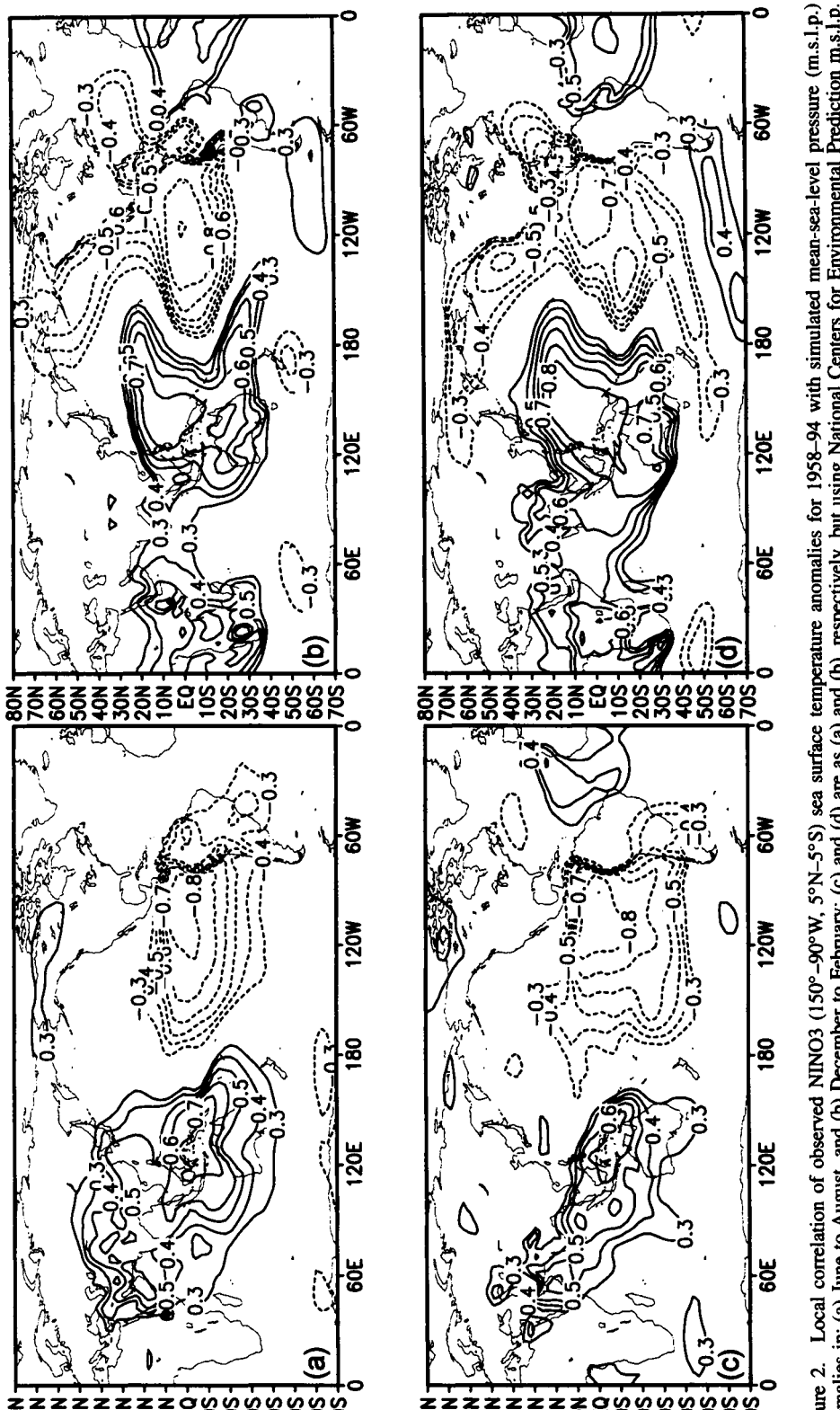

Figure 2. Local correlation of observed NINO3 (150°–90°W, 5°N–5°S) sea surface temperature anomalies for 1958–94 with simulated mean-sea-level pressure (m.s.l.p.) anomalies in: (a) June to August, and (b) December to February; (c) and (d) are as (a) and (b), respectively, but using National Centers for Environmental Prediction m.s.l.p. re-analyses. Only absolute values greater than 0.3 are shown, which are significant at the 95% level.

Chile to New Zealand and a positive band to the south are found in the re-analyses. These structures are also simulated by the model, but with somewhat reduced amplitudes.

Figures 3(c) and (d) show the correlation of the NINO3 SSTA with T_{850hPa} derived from the NCEP re-analyses for JJA and DJF, respectively. In JJA, strong positive ENSO connections are found over the central and eastern Pacific, the Caribbean, southern Brazil and India, while an inverse relationship occurs over north-eastern Australia and the adjacent South Pacific, the Sea of Okhotsk and along the coast of California. In DJF, positive correlations are observed over the central and eastern Pacific, northern South America, the Caribbean, the tropical and subtropical Atlantic, southern Africa, the Indian Ocean, north-eastern Australia, the Chinese Sea and Canada, while large negative values are found over the North Pacific, the southern USA and east of the Philippines. For areas where land stations exist, these figures resemble those given by Halpert and Ropolewski (1992).

In JJA the model captures the ENSO-related anomalies over the tropical Pacific, the Caribbean, India, and southern Brazil (Fig. 3(a)). However, it simulates a positive relationship over northern South America, which is unrealistic. Moreover, the band of negative correlations in the western South Pacific does not cover north-eastern Australia as is observed. A weak correlation pattern is simulated over the North Pacific but, contrary to the re-analyses, it is located over the centre of the basin. In DJF the simulated T_{850hPa} teleconnection pattern is in remarkable agreement with the re-analyses (Fig. 3(b)). At lower latitudes the only difference is found over north-eastern Australia. The simulated PNA pattern seems quite realistic, only the positive link to Canada is too strong. The model gives some negative correlations in the South Pacific between New Zealand and Chile, and positive values southward. These are slightly indicated in the re-analyses too, but the numbers are relatively small and not significant.

The simulated rainfall teleconnection patterns (Fig. 4(a) and (b)) are quite realistic over the tropical Pacific and the Americas, while the results are much less satisfactory in other regions. Consistent with Ropolewski and Halpert (1987), the Hulme rainfall data for JJA yield positive correlations over the central Pacific and the north-western USA, and negative ENSO correlations over Indonesia, eastern Australia, the south-western Pacific, north-eastern South and Central America, and India (Fig. 4(c)). Moreover, the Hulme dataset shows some negative correlations over northern Africa and China. The model fails to simulate the observed teleconnections over the north-western USA, eastern Australia, and China. The simulation of the Indian monsoon/ENSO relationship is also unrealistic. Moreover, the negative anomaly pattern over the Indonesian area is only weakly simulated by the model, and intersected by a positive band which extends into the Indian Ocean.

The rainfall teleconnection patterns derived from the Hulme data for DJF (Fig. 4(d)) resemble those known from Ropolewski and Halpert (1987) except over the Chinese Sea and the north-western USA, where they show additionally a positive and negative relationship, respectively. Rainfall anomalies in eastern equatorial Africa are not prominent in this dataset during DJF. The model captures the positive correlations over the central Pacific, the southern USA and Mexico, and the Chinese Sea; it also captures the negative relationships north and south of the equatorial Pacific rainband, over northern South America and the north-western USA. However, the simulated equatorial Pacific rainfall anomalies do not touch South America as is observed. This problem is related to model resolution and orography, and can be solved by applying a higher model-resolution (T106; Merkel, personal communication). The simulated ENSO impact over the Indonesian archipelago is too weak, and the influences on eastern Australia and southern Africa are totally missing.

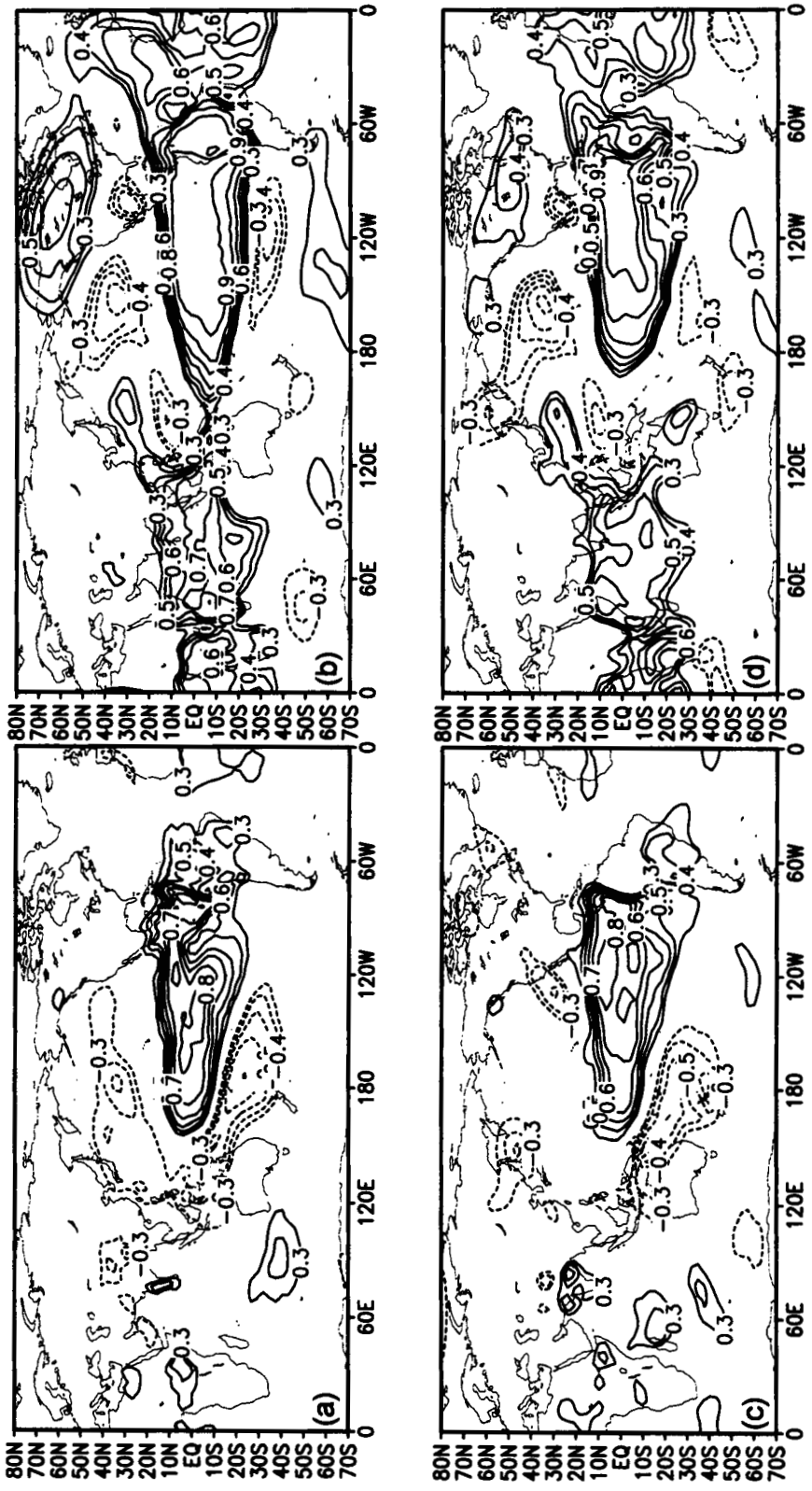

Figure 3. As Fig. 2 but for simulated 850 hPa temperature anomalies in (a) and (b), and re-analysis values in (c) and (d).

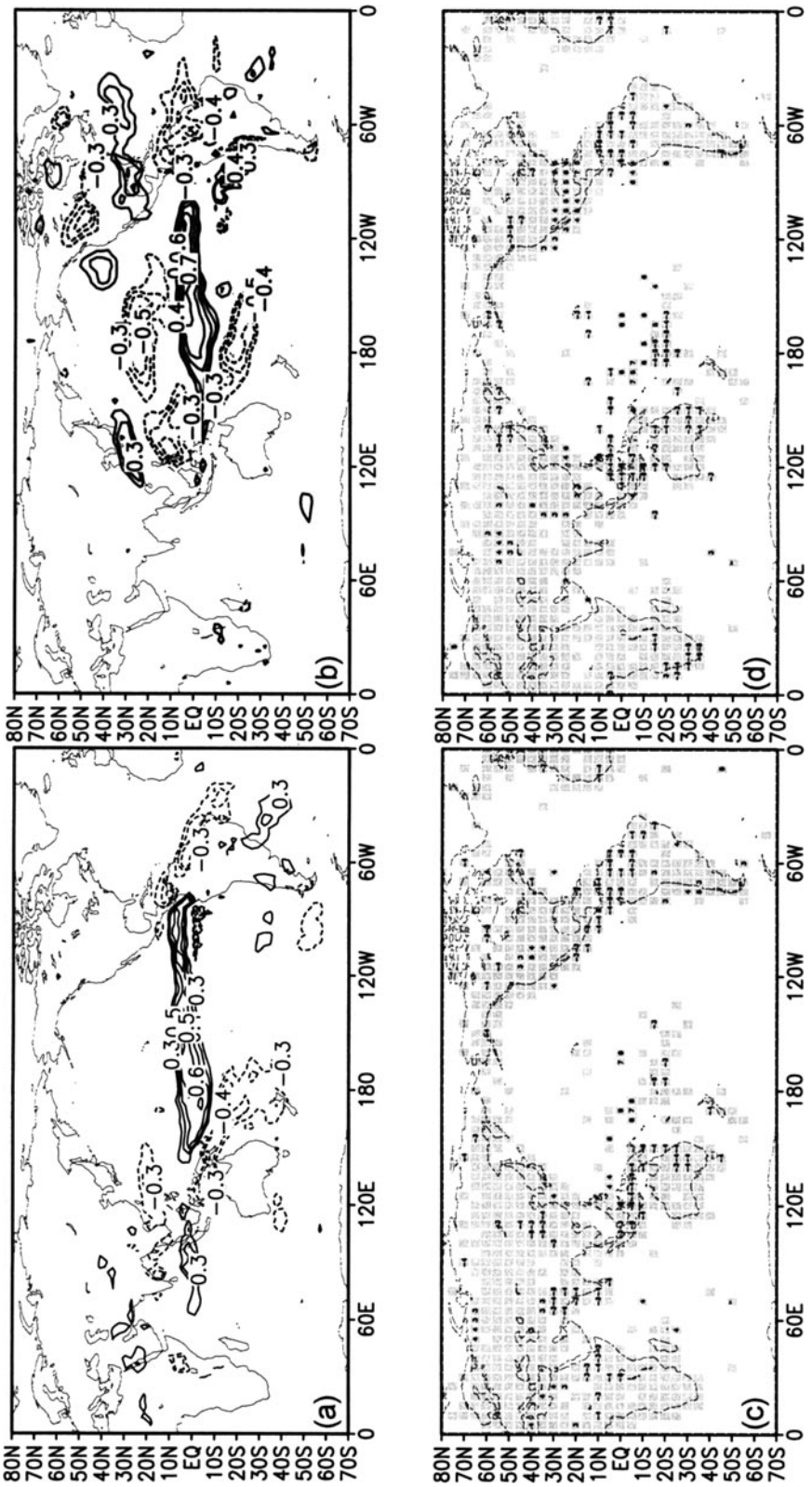

Figure 4. As Fig. 2 but for simulated rainfall anomalies in (a) and (b), and observed rainfall anomalies in (c) and (d). Correlation coefficients for observations have been multiplied by 10 for plotting. In (c) and (d) shading marks areas where measurements are available.

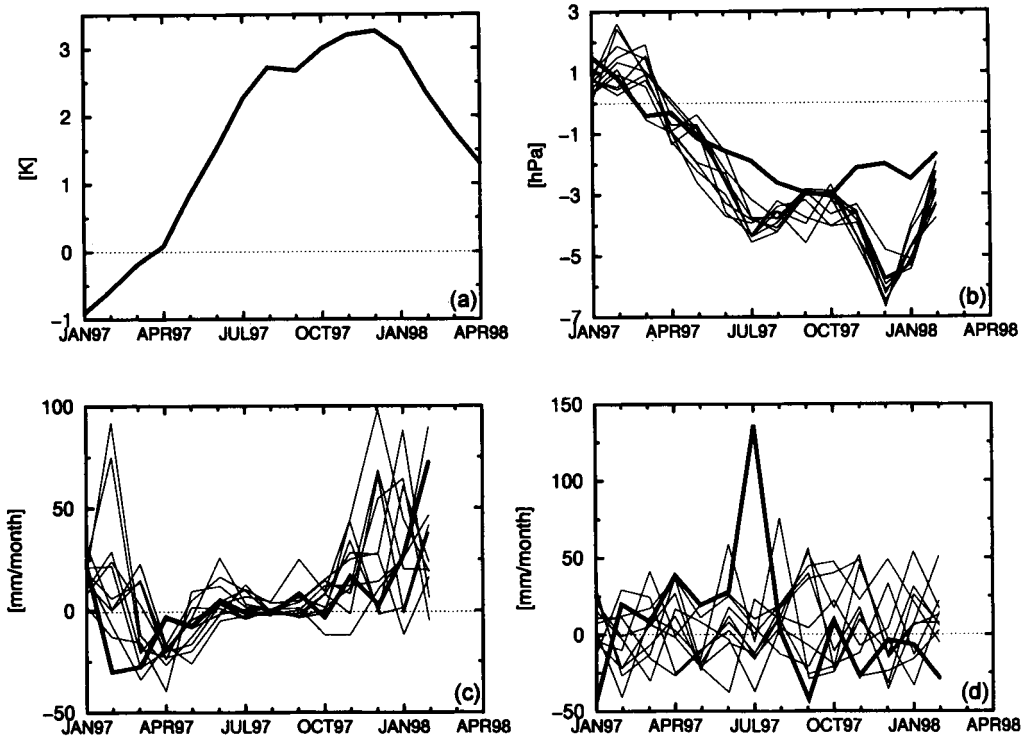

Figure 5. Time series from January 1997 to February 1998 inclusive of: (a) NINO3 area (150°–90°W, 5°N–5°S) sea surface temperature anomalies (degC); (b) an equatorial (130°–80°W, 5°N–5°S minus 90°–140°E, 5°N–5°S) Southern Oscillation Index (hPa); (c) rainfall anomalies (mm month^{-1}) over California (110°–125°W, 30°–45°N); and (d) rainfall anomalies over eastern central Europe (10°–20°E, 45°–55°N). The thin lines show the simulated ensemble trajectories for the globally forced experiment while the observations are given by the thick line.

4. ATMOSPHERIC RESPONSE TO GLOBAL SSTAS IN 1997/98

Time series of observed and simulated anomalous equatorial Southern Oscillation indices (SOIs) and anomalous precipitation over selected regions are shown in Fig. 5. The eastern Pacific SSTA expressed by the NINO3 index is shown for comparison (Fig. 5(a)). The observed SOI decreased very rapidly early in 1997, consistent with the tropical SST forcing (Fig. 5(b)). However, while the NINO3 anomaly reached its maximum in December, the Southern Oscillation attained its minimum in October and increased thereafter. Although the SSTAs were of comparable amplitude to those observed during the strong 1982/83 event, the SOI response reached only 3/4 of the 1982/1983 event. The simulated ensemble trajectories show the same rapid drop from spring to autumn as the observations. The spread within the ensemble is quite small, illustrating the low noise level of the tropical atmosphere. The model does not simulate the early increase of the SOI starting in October but attains a minimum value of about −6 hPa in December, as expected from the NINO3 SSTA. However, this consistency probably occurs for the wrong reason, since the model generally reacts too strongly to tropical Pacific SSTAs.

The high level of reproducibility of tropical circulation anomalies is not found over other regions of the globe or for other variables. California, for instance, experienced anomalously wet conditions in winter 1997/98 due to a southward shift of the storm track. The simulated Californian rainfall anomalies for 1997/98 (Fig. 5(c)) show a much

TABLE 1. PATTERN CORRELATIONS OF SIMULATED ENSEMBLE MEAN AND OBSERVED ANOMALIES FOR EL NIÑO 1997/98 FOR SELECTED REGIONS

	m.s.l.p.		T_{850hPa}		P	
	JJA	DJF	JJA	DJF	JJA	DJF
Global	**0.44 (0.36)**	**0.78 (0.37)**	**0.58 (0.21)**	**0.73 (0.25)**	**0.41 (0.04)**	**0.59 (0.06)**
Tropics	**0.74 (0.49)**	**0.87 (0.43)**	**0.67 (0.38)**	**0.73 (0.31)**	**0.42 (0.05)**	**0.59 (0.07)**
N. hem.	−0.03 (0.45)	**0.90 (0.55)**	0.13 (0.37)	**0.77 (0.39)**	−0.13 (0.10)	**0.65 (0.21)**
S. hem.	0.40 (0.52)	0.42 (0.46)	**0.66 (0.36)**	**0.61 (0.45)**	**0.41 (0.18)**	**0.40 (0.15)**
PNA	−0.32 (0.66)	**0.94 (0.70)**	0.16 (0.59)	**0.80 (0.69)**	−0.09 (0.27)	**0.68 (0.26)**

The numbers in brackets give confidence limits according to the criteria given in the text. Significant values are in boldprint.

larger scatter relative to the SOI. There is, however, a clear tendency for enhanced rainfall in winter 1997/98, consistent with the observations. This is totally different over eastern central Europe (Fig. 5(d)), where the simulated trajectories do not show any common signal. This is true also for July 1997, when heavy rainfall caused severe flooding in eastern Germany and Poland. Although a summer ENSO teleconnection to Europe has not so far been reported in the literature, there has been much speculation, especially in the press, about a causal link to El Niño in 1997. Indeed, a model simulation performed by Stockdale *et al.* (1998) supports this assumption. Our model simulations do not support the conclusion that the flooding over eastern Europe was caused either by El Niño or by other non ENSO-related SSTAs.

The global response of the ECHAM4 model is illustrated by ensemble-mean anomaly maps of m.s.l.p., T_{850hPa}, and P in Figs. 6 to 8. The maps are compared with observations given by the NCEP re-analysis and CAMS/OPI data. Regions which exhibit a significant response in the simulations are indicated by shading. The simulated response patterns will be compared with the teleconnection patterns shown in Figs. 2 to 4. The agreement between the model simulations and observations should be considered with caution, because an ensemble mean represents a smoothing while the observations reflect just one realization of many possibilities. The comparison of simulated and observed anomalies will be carried out primarily by visual inspection of the response patterns. However, in order to give a more objective measure of the agreement between model and observations, pattern correlations of the respective anomaly fields have been calculated for selected regions of interest. These are shown in Table 1 for the whole globe, the entire tropics (30°N–30°S), the extratropical northern (30°–70°N) and southern (30°–70°S) hemispheres, and the PNA region (0°–180°W, 30°–70°N) for both JJA and DJF. One has to put confidence limits on these estimates since high correlations could also occur by chance. A rigorous significance test for the pattern correlation coefficients is not straightforward, since the estimation of spatial degrees of freedom is rather complicated. As an alternative approach, the observed anomaly patterns have been correlated with the 26 realizations of the climatologically forced experiment containing only anomalies arising from the internal variability of the atmosphere. The resulting frequency distributions (not shown) provide the range of correlation caused by internal random noise. We have chosen the maximum values occurring within these frequency distributions as thresholds to decide whether a pattern correlation is significant or not. Such a procedure does not represent a rigorous test, but at least yields an indication of the reliability of the derived pattern correlations.

The main m.s.l.p. signal (Fig. 6) is the signature of the Southern Oscillation, with negative anomalies in the east Pacific and positive values over the Indonesian region in both northern hemisphere summer (JJA) and winter (DJF). The western part of the

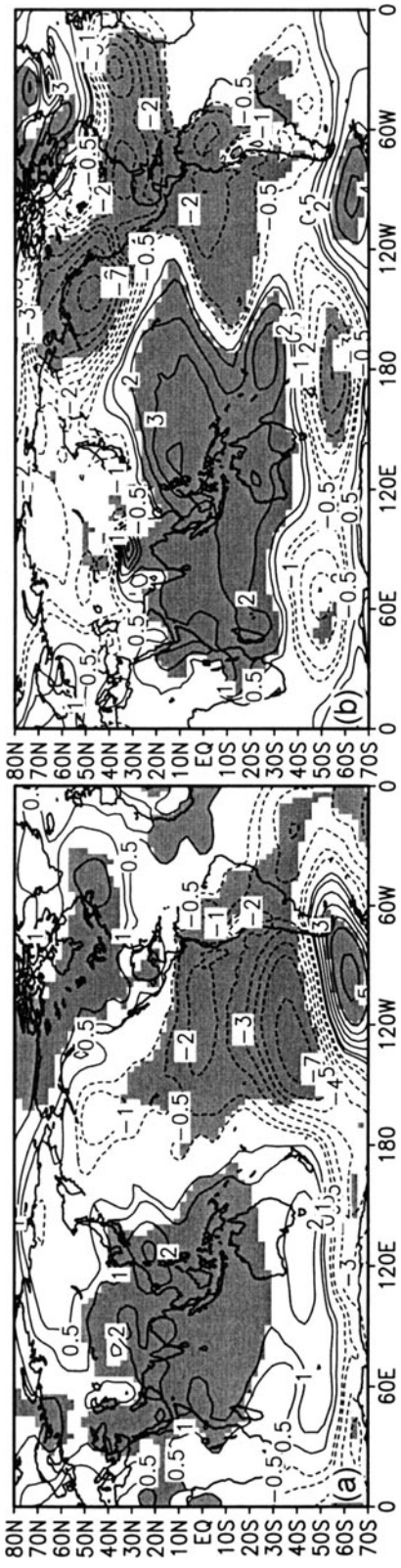

Figure 6. Ensemble mean-sea-level pressure (m.s.l.p.) anomalies (hPa) for (a) June to August 1997, and (b) December to February 1997/98 derived from the globally forced experiment; (c) and (d) are as (a) and (b) but for m.s.l.p. anomalies taken from the re-analysis data. Contour lines are shown for ±0.5, 1, 2, 3, 4, 5, 7, 9, 12 hPa. Areas with a statistically significant signal (99% confidence level) have been shaded in the model plots.

Pacific signal covers quite a large area including northern Australia and extending far into the Indian Ocean. These features are found both in the model results and in the re-analyses, but with differing amplitudes in the eastern Pacific as already mentioned above. Moreover, two pronounced high-pressure anomalies are found on both sides of the equator in the western Pacific in DJF in both the model and re-analyses. The simulation yields a pronounced positive pressure anomaly over the Indian subcontinent in JJA, which was not observed. However, this result cannot be trusted, since the model generally overestimates m.s.l.p. teleconnections over south-east Asia (Fig. 2(a) and (c)).

The link of ENSO to the extratropics is strongest in the winter hemisphere due to the stronger meridional potential-vorticity gradients. A pronounced southern Pacific wave train, with negative anomalies in the subtropics and an anomalous high west of the Drake passage, is simulated in JJA. At least the negative centre is also found in the observations. It is not clear if the observed anomalous southern ocean high can be linked to a Rossby wave train originating in the tropics, since it is displaced too far westward. A link of El Niño to the southern ocean in JJA cannot be established from previous ENSO events, either in the NCEP re-analyses or in the long-term GISST experiments (Fig. 2). However, no El Niño during 1958 to 1994 exhibited as strong an amplitude in JJA as that in 1997. Thus, it seems plausible that the simulated and analysed southern ocean anomalies can be attributed to the unique evolution of the 1997/98 El Niño and not to internal variability of the atmosphere. Some indications of a systematic response are simulated in the northern hemisphere during JJA, probably also related to the early peaking of the 1997/98 El Niño. The pressure is lower over the North Pacific and enhanced over North America, in some respects resembling the PNA pattern. However, this signal is weak, and is only significant over North America (the northern Pacific negative centre is only significant at the 95% level) and not present in the observations.

In winter (DJF), a well developed PNA pattern is found in both the model simulation and the observations. The Aleutian low is intensified, positive anomalies are found over northern Canada and Greenland, and a negative anomaly extends from the USA across the North Atlantic to the European coasts. In the statistics of previous ENSOs significant teleconnections over the North Atlantic are restricted to the south-western part of the basin (Fig. 2), both in the model and the re-analyses. However, both the simulated and analysed m.s.l.p. anomaly fields for 1997/98 can be viewed as an intensification and north-eastward extension of these statistically derived patterns, and are probably related to the extraordinary strength of the 1997/98 event. Contrary to the summer conditions, where no signal was found over Europe, these wintertime anomalies over the North Atlantic also had an impact on Europe: the North Atlantic jet was split into two branches; the southern branch carried warm and moist air masses to western Europe; the northern part was responsible for the severe winter in eastern Europe. This configuration is very similar to results found in a modelling study reported by Palmer and Anderson (1994), but does not share many similarities with a statistical analysis of El Niño impacts in Europe described by Fraedrich and Müller (1992). Although the simulated North Atlantic anomalies cover the entire basin, the impact on Europe, at least as far as pressure is concerned, is not significant and does not resemble the re-analyses. Obviously, even for such a strong event, any systematic response over Europe cannot be detected against the strong internal variability. A clear signal is also found in the southern hemisphere in DJF in the model results. Significant anomalies are simulated, with three centres covering almost the entire southern ocean. The positive anomaly west of the Drake passage is also found in the re-analysis. Since this positive pattern also appears in the teleconnection maps given in section 3 (both for model and re-analysis)

it must be regarded as a systematic response to ENSO, which will be further clarified in the next section.

The overall resemblance of simulated and analysed m.s.l.p. anomaly fields is limited to the tropics during JJA (Table 1), where the pattern correlation is 0.74. For the extratropical regions under consideration the pattern correlations are rather low, and do not exceed the significance threshold mentioned above. In DJF clear pattern resemblance is also found over the northern hemisphere extratropics. Both in the tropics and extratropics the pattern correlations exceed 0.8 and, especially in the PNA area, the ECHAM4 model reveals a remarkable skill of more than 0.9. The resemblance of southern hemisphere anomalies is much weaker and does not exceed the significance threshold.

Instead of near-surface temperature, which is strongly influenced by local effects and therefore more difficult to simulate, 850 hPa temperature anomalies (Fig. 7) effectively represent the large-scale temperature response. During JJA 1997 the response was mainly confined to the tropics. The model results show the direct heating over the eastern Pacific which extends over northern South America and Central America, while north of Australia and within the region of the South Pacific convergence zone a significant cooling is simulated. As is the case for previous El Niños, the model overestimates the warming over northern South America. Other significant warmings are simulated over the tropical Atlantic, India, eastern Africa, and parts of the southern ocean. None of these was observed in 1997/98, and only the warming over India represents a systematic teleconnection known from previous El Niños.

During DJF 1997/98, when the equatorial SSTAs were strongest, significant temperature anomalies are simulated in many places. The simulated warming now covers almost the entire tropics. It is not surprising that the warming is strongest over the eastern Pacific, but South America, the tropical Atlantic, Africa, the Indian Ocean, and southeast Asia also experienced a significant warming. These tropical anomaly structures are consistent with historical teleconnection patterns (Fig. 3(b) and (d)) and are similar to the observed anomalies in 1997/98. The correlation of the tropical patterns in DJF amounts to 0.73 (see Table 1).

The strongest extratropical signal during DJF 1997/98 is related to the PNA pattern. In both the model and the observations, intensified cold-air advection associated with the anomalously strong Aleutian low cooled the North Pacific atmosphere. The southward shift and eastern intensification of the Pacific jet stream caused lower temperatures over the southern USA. The shift of the standing-wave pattern over North America resulted in strongly reduced cold-air advection and gave rise to the record temperatures over Canada and the northern USA. These temperature anomalies are well captured by the model, the pattern correlation amounting to 0.8. Furthermore, they can be directly attributed to El Niño, since the teleconnection patterns from previous ENSO events reveal almost the same structure (Fig. 3(b) and (d)). The observed wintertime temperature anomalies over Europe—mild in the west, very cold in the east—are also reproduced in the ensemble experiments. However, only the warm signal over western Europe is significant and systematically related to ENSO, as shown by the hindcast patterns (Fig. 3(b) and (d)). For eastern Europe the model does not show any hindcast skill for $T_{850\text{hPa}}$, and the cooling in 1997/98 cannot be separated from internal noise. The simulated DJF warming over China is apparently a model artifact since it was neither observed nor does it represent a known teleconnection. However, the model is able to capture the observed temperature anomalies over the southern Pacific which are at least weakly connected to the tropics, as the simulated and analysed teleconnection patterns (Fig. 3(b) and (d)) reveal. Nevertheless, an impact of the southern ocean itself cannot be excluded at this

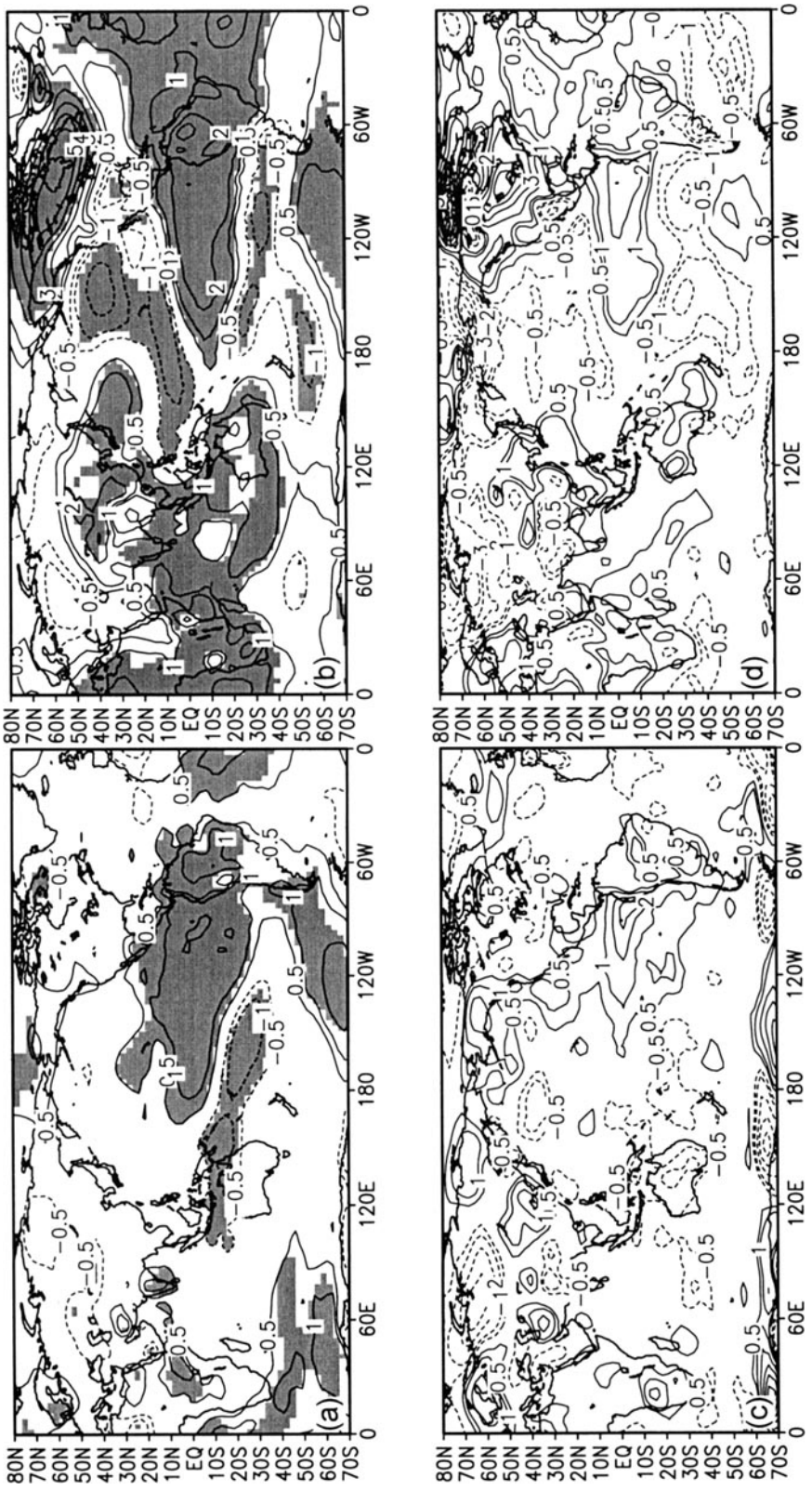

Figure 7. As Fig. 6 but for 850 hPa temperature anomalies (degC).

point, since the respective SSTAs (Fig. 1(b)) in this area reveal a structure quite similar to that found at 850 hPa.

The overall skill for $T_{850\text{hPa}}$, as given by the pattern correlations in Table 1, is generally lower than for m.s.l.p. However, except for the northern hemisphere in JJA, where the pattern correlations do not exceed the significance thresholds, the simulation results are still in reasonable agreement with the re-analyses. Here the pattern correlations generally exceed 0.6. The model results appear to be rather skilful, especially for the PNA region in winter where the correlation is 0.8.

The simulation of precipitation is much more difficult than the other two variables. Rainfall depends on small-scale processes and is strongly influenced by the chaotic nature of atmospheric weather fluctuations. Thus, it is not surprising that the systematic rainfall response simulated in the ensemble integrations is mainly confined to the tropics and subtropics, while significant signals in mid latitudes are almost absent. Furthermore, even at lower latitudes the simulation of the precise location of rainfall anomalies is difficult, as the comparison of the model results with the CAMS/OPI data indicates (Fig. 8).

Although the El Niño SSTA was already well-developed in JJA 1997, the intense eastern Pacific rainfall anomalies did not touch South America at this time of the year either in the model simulation or in the observations (Fig. 8(a) and (c)). As expected from the teleconnection patterns (Fig. 4(a) and (c)), the model captures the observed dry anomalies over the South Pacific convergence zone, Indonesia, the Indian Ocean, and the Chinese Sea. However, as pointed out in section 3, the simulated dry anomalies are intersected by an erroneous wet band over the Indian Ocean. No reduction of Indian monsoon rainfall was apparent in JJA 1997, while the model simulated drier conditions over India. This difference is likely to be due to model deficiencies, since ECHAM4 possesses little skill over India anyway. As expected from previous El Niños, the simulated dry anomalies over Central America, northern South America, and the tropical Atlantic are quite realistic. Whether the dry anomalies over the tropical Atlantic were related only to the extraordinary strength of El Niño in JJA 1997 or to the cold SSTAs in the tropical Atlantic itself (Fig. 1(a)) remains unclear. The wet anomalies over Chile extending westward over the Pacific must be regarded as a robust feature, since they are found both in the model and in the data in JJA of 1997 and during other El Niños.

Both the model and observations show a dramatic increase in rainfall over the eastern Pacific in DJF 1997/98. The model simulations yield values about twice as large as the CAMS/OPI analyses. This can be attributed partly to the excessive sensitivity of the ECHAM4 model to eastern Pacific SST anomalies. However, the measured values are much too low, since the satellite algorithm was not able to record the very strong anomalies in DJF 1997/98 correctly (J. Janowiak, NOAA CPC, personal communication). The simulated wet anomalies do not cover Peru and Ecuador where intense rainfall caused severe flooding. This failure may be attributable to the relatively coarse resolution of our model, which does not resolve the steep orography in this region well. The dry conditions over the western Pacific, north and south of the equatorial rainband, and in the western Indian Ocean are simulated. However, the unrealistic intersecting narrow band of enhanced precipitation is again depicted over the western Indian Ocean. The model reproduces the observed rainfall anomalies over Central and northern South America, Florida, the western North Atlantic, and south of Japan. All these regions exhibit considerable skill in the simulations of previous ENSO extremes (Fig. 4(b) and (d)). California usually did not experience systematic precipitation anomalies related to ENSO in DJF (Ropolewski and Halpert 1987; Fig. 4(b) and

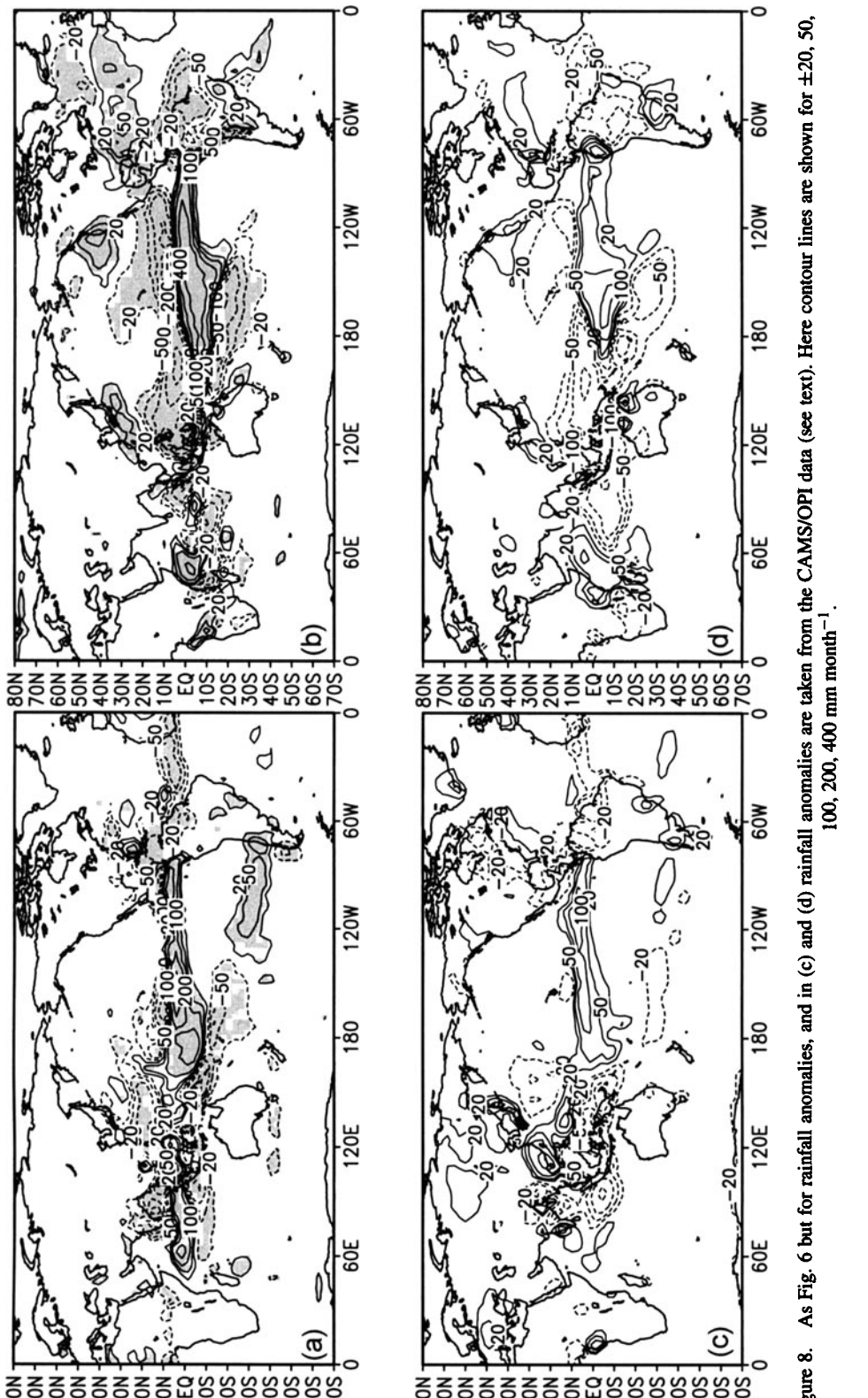

Figure 8. As Fig. 6 but for rainfall anomalies, and in (c) and (d) rainfall anomalies are taken from the CAMS/OPI data (see text). Here contour lines are shown for ±20, 50, 100, 200, 400 mm month^{-1}.

(d)). However, winter 1997/98 was characterized by rainfall twice as large as normal. Since these rainfall anomalies are reproduced by the ensemble mean of the model experiments, it is very likely that they must be attributed to the unusual strength of El Niño 1997/98. The simulations of previous ENSO extremes do not show any skill over southern Africa and north-eastern Australia (Fig. 4(b)). Hence, it is not surprising that the observed reduced rainfall over southern Africa could not be simulated. Over north-eastern Australia, drier than normal conditions did not occur in DJF 1997/98. The model shows the same behaviour, but probably due to the wrong reason since it generally fails to simulate the negative ENSO-related rainfall anomalies over this region. Although a teleconnection to equatorial eastern Africa does not show up in our analyses of previous ENSO extremes, intense rainfall anomalies were observed over this region and the adjacent ocean. Eastern African rainfall anomalies are in general closely linked to SSTAs in the Indian Ocean (Rocha and Simmonds 1997; Goddard and Graham 1999), and the excess in rainfall over eastern Africa and the Indian Ocean in DJF 1997/98 must be also attributed to the exceptionally strong SSTAs in the Indian Ocean itself (Latif *et al.* 1999). However, our model simulations only capture the precipitation enhancement over the ocean; they fail to simulate the intense rainfall anomalies over eastern equatorial Africa.

In summary, the agreement between observed and simulated rainfall anomalies is rather poor for JJA 1997 (Table 1). Pattern correlations hardly exceed 0.4 and are not significant for the northern hemisphere and the PNA region. For DJF 1997/98, the observed and simulated patterns are more similar. In spite of the problems in the Indian Ocean sector, the tropical patterns are still correlated at 0.59. Over the PNA sector the results are even better, with a pattern correlation coefficient of 0.68.

5. Atmospheric response to regionally confined SSTAs

Most of the circulation anomalies observed during the 1997/98 El Niño are in agreement with the teleconnections seen in previous El Niño events. However, some marked deviations also occurred. For example, DJF 1997/98 was characterized by strong circulation anomalies covering the entire North Atlantic which were accompanied by warm and moist conditions over western Europe; these anomalies are well captured by the model. It is well known that El Niño has some influence on the North Atlantic area, and a weak link of European wintertime climate to El Niño conditions has been reported by Fraedrich and Müller (1992). However, the observed 1997/98 wintertime circulation anomalies were much stronger than expected from the canonical ENSO teleconnection pattern, and did not resemble the patterns of Fraedrich and Müller (1992). To investigate whether such deviations were caused by the extraordinary strength of El Niño 1997/98 in the Pacific or by other SSTAs, further model experiments have been performed in which the SSTAs were restricted to either the Pacific or Atlantic Ocean.

These experiments show that the global response of the atmosphere in DJF 1997/98 was largely related to Pacific SSTAs. Nearly the entire m.s.l.p. response structure of the globally forced experiment (see Fig. 6) is reproduced by the Pacific-only experiment (Fig. 9). Even the amplitudes, and small-scale structures such as the pressure anomalies over the Himalayas and South Africa, are captured by the Pacific-only experiment, confirming the statistical reliability of ten realizations. The response over the North Atlantic with high pressure over Greenland and low pressure in the subtropics is also fully reproduced by the Pacific-only experiment. The pressure anomalies obtained in the Atlantic-only experiment do not show any systematic response over the entire globe. Interestingly, the wave-like structure over the southern ocean described above

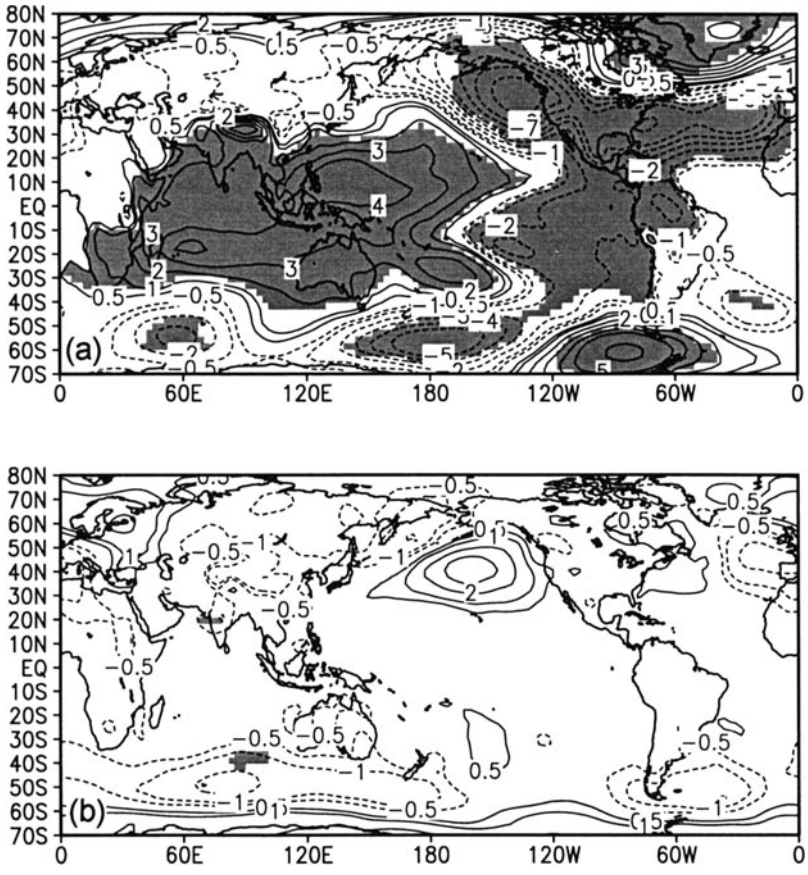

Figure 9. Ensemble mean-sea-level pressure anomalies (hPa) for December to February 1997/98 for: (a) the Pacific-only experiment, and (b) the Atlantic-only experiment. Contour lines are shown for values: ±0.5, 1, 2, 3, 4, 5, 7, 9 and 12. Areas with a statistically significant signal (99% confidence level) have been shaded in the model plots.

is captured by the Pacific-only experiment, although no SSTAs were prescribed south of 30°S. This indicates a link between the southern hemispheric mid-latitude circulation and El Niño, which might have important implications for the Antarctic circumpolar wave (White and Peterson 1996; Christoph *et al.* 1997).

The Pacific-only experiment also reproduces most anomalies in the 850 hPa temperature fields (Fig. 10) which were found in the experiment with globally prescribed SSTs. Only the temperature signal over the Indian Ocean is not reproduced; this can be attributed to the large Indian Ocean SSTAs (see Fig. 1(b)) which were present in winter 1997/98; the origin of these anomalies is not clear. Webster *et al.* (1999) argue that they might have been caused by an inherent Indian Ocean coupled air–sea mode involving equatorial waves, atmospheric convection, and the monsoon. On the other hand, it is known that Indian Ocean SSTs are statistically linked to El Niño (Pan and Oort 1983; Venzke *et al.* 1999). Our Pacific-only experiment yields heat-flux anomalies over the Indian Ocean (not shown; Latif *et al.* 1999) with structure and sign suitable for creating the observed SSTA pattern. Thus, the Indian Ocean SSTAs and lower-tropospheric temperature anomalies may represent a response to ENSO. The warm $T_{850\text{hPa}}$ anomalies

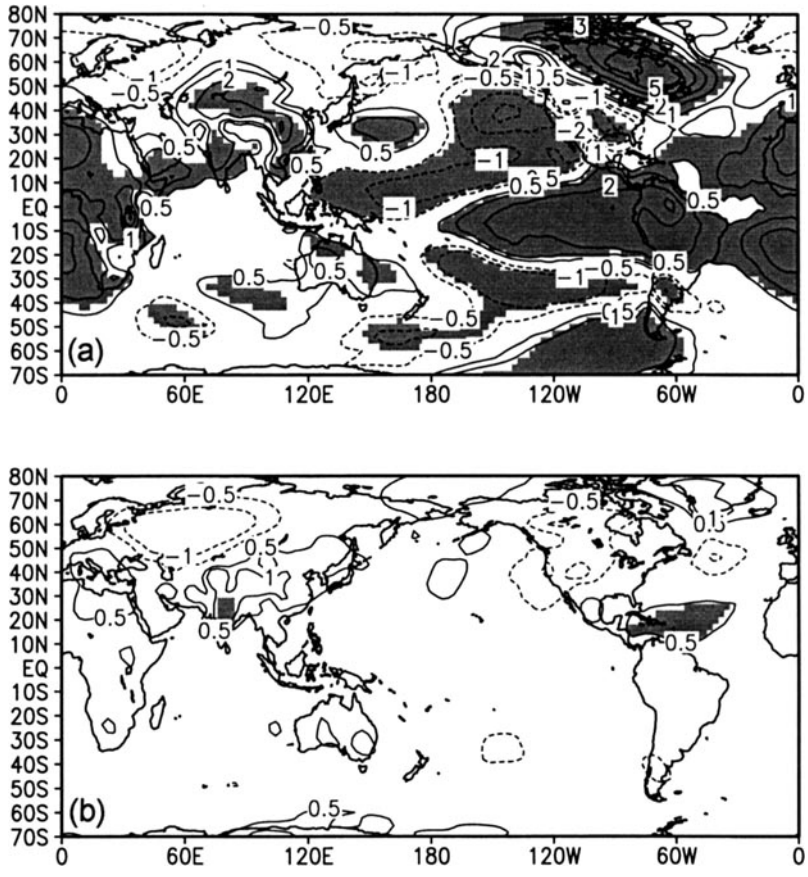

Figure 10. As Fig. 9 but for 850 hPa temperature anomalies (degC).

west of the Drake Passage in DJF 1997/98 are also apparent in the Pacific-only experiment. Warm air masses were transported by anomalous geostrophic advection (Fig. 9(a), Fig. 6(b) and (d)) into that region. Once again, the Pacific-only experiment yields heat-flux anomalies suitable for creating the SSTAs. Thus, these atmospheric temperature anomalies can be attributed to the anomalous circulation during this time and not to the underlying SSTAs. In addition, the SSTAs are apparently created by the anomalous atmospheric forcing. The Atlantic-only experiment yields a significant temperature response of about 0.5 degC only over the western subtropical Atlantic (Fig. 10(b)) downstream of the main SSTAs. This response can be attributed to the direct heating of the boundary layer from below.

Although systematic rainfall anomalies are statistically much less robust, the overall global rainfall anomaly pattern of the globally forced experiment is well captured by the Pacific-only experiment (Fig. 11(a)). Although the North Atlantic rainfall anomalies appear to be mainly forced by the Pacific, a smaller but significant impact by local SSTAs was simulated. The Atlantic-only experiment (Fig. 11(b)) yields a significant increase of precipitation over the tropical Atlantic, parts of Central America, and over parts of northern Africa and southern Europe. This suggests that Atlantic SSTAs are not negligible in simulating and predicting regional climate anomalies.

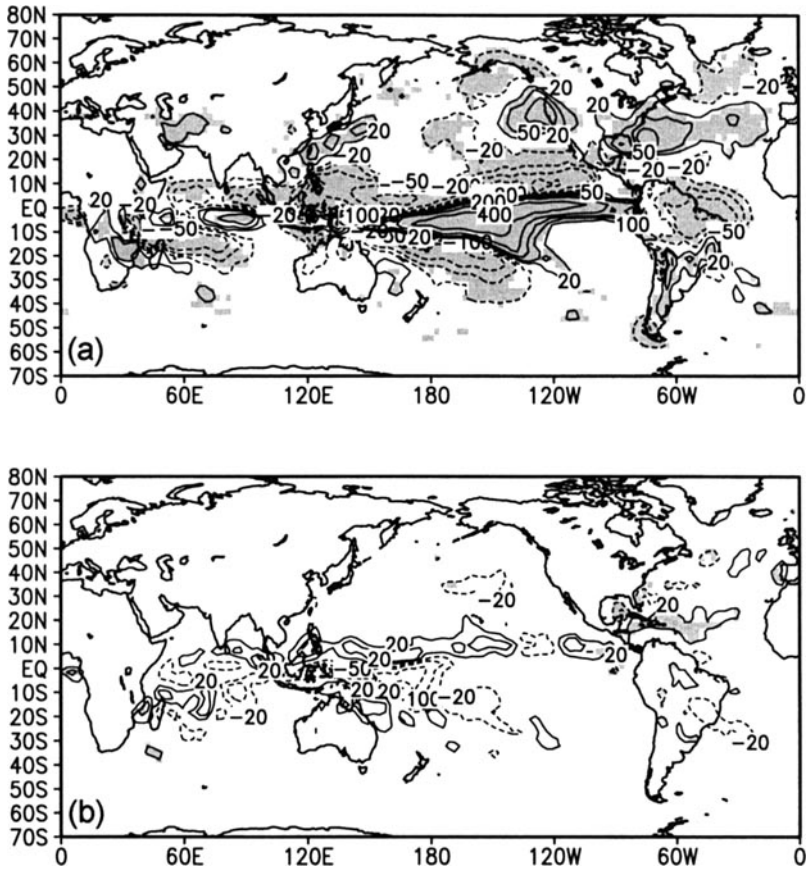

Figure 11. As Fig. 9 but for rainfall anomalies. Here contour lines are shown for ±20, 50, 100, 200, 400 mm month^{-1}.

6. Summary and Conclusions

Ensemble integrations with the ECHAM4 AGCM forced by observed SSTs have been performed to investigate the global atmospheric response to the 1997/98 El Niño. To a large extent the climate anomalies observed in 1997/98 fit into the canonical ENSO teleconnection picture and are reproduced by the model. These anomalies include the signature of the Southern Oscillation, the tropical temperature anomalies, the wet and dry anomalies over the tropical Pacific and northern South America, as well as the enhanced rainfall over Florida, the western North Atlantic and equatorial East Africa. This is also the case for the PNA pattern and the link to the southern ocean in DJF, which was simulated quite realistically. Altogether, the model results are quite realistic over the Pacific, the Americas, and the Atlantic, while the performance over the Indian Ocean and the adjacent land masses is much less satisfactory. During JJA the model skill is more or less confined to the tropics. During DJF considerable correspondence to the observations could also be obtained for the extratropics, especially for the PNA sector. However, the model Walker cell responds too strongly to anomalous SST forcing. The eastern Pacific rainfall anomalies do not reach South America due, in part, to the coarse resolution of the model as shown by integrations at higher resolution. The heating over northern South America is overestimated. Moreover, the model simulates an unrealistic rainband

over Indonesia, and it fails to reproduce the El Niño related precipitation anomalies over southern Africa.

Not all the climate anomalies observed in 1997/98 were expected from known ENSO teleconnections. The circulation anomalies over the North Atlantic were much stronger than usual. Since they were successfully simulated by the model, it is likely that they can be attributed to the enormous strength of this particular El Niño event and not to internal variability. The same seems to be the case for the circulation anomalies over the southern ocean in JJA and for the intense rainfall anomalies over California in DJF 1997/98. However, no systematic response over Europe, neither in winter nor summer, could be established from our model results both for the 1997/98 El Niño and previous ENSO events. The hypothesis that the summer flooding over eastern Central Europe was related to the early peaking of El Niño in 1997 is not supported by our model experiments. However, this result should be viewed with caution since the model does not show any skill over Europe for previous El Niños, and the hypothesized impact on Europe in 1997 due to the large amplitude of the 1997/98 El Niño event might be underestimated due to model deficiencies. No clear conclusions can be drawn for the more or less normal monsoon rainfalls over India and north-eastern Australia compared with other El Niño years, since the model performance is too poor over those regions. Further experiments restricted to particular ocean basins have shown that most of the systematic atmospheric climate anomalies in 1997/98 were related to Pacific SSTAs. In particular, Atlantic SSTAs had only a regional impact on the atmosphere.

Most of the climate anomalies observed in 1997/98 were in agreement with expected ENSO teleconnections, but our model experiments indicate that some of the deviations might be related to the unusual strength and time evolution of this particular event. Some unexpected climate anomalies during 1997/98 could not be related either to anomalous SST forcing or to internal atmospheric variability, since the model cannot be trusted over certain regions. Further model development, experiments and comparisons with other models will be required to clarify these points. The simulation of orographically related precipitation within the ECHAM4 model will benefit from a higher model resolution, while an improved simulation of the monsoon rainfall is expected from a more refined land surface scheme (Schulz, personal communication). The unrealistically strong sensitivity of the model Walker cell is probably related to the fact that the model simulates too much convection over the warm pool and too little over the eastern Pacific. This problem can probably be resolved by a refined closure and tuning of the cumulus convection scheme. These and other model improvements are underway.

ACKNOWLEDGEMENTS

The re-analysis data and the CAMS/OPI precipitation estimates were provided by NCEP. The Reynolds SST forcing data were kindly given by the NOAA Climate Diagnostics Centre. This work was supported by the European Union's PROVOST (ENV4-CT95-0109) programme and the German government under its programme 'Klimavariabiliät und Signalanalyse'. The AGCM integrations were performed at the Deutsches Klimarechenzentrum. We would also like to thank the two anonymous reviewers for making valuable comments and suggestions.

REFERENCES

Anderson, J., van den Dool, H., Barnston, A., Chen, W., Sternamd, W. and Ploshay, J. 1999 Present-day capabilities of numerical and statistical models for atmospheric extratropical seasonal simulation and prediction. *Bull. Am. Meteorol. Soc.*, **80**, 1349–1362

Barnett, T. P., Bengtsson, L., Arpe, K., Flügel, M., Graham, N., Latif, M., Ritchie, J., Roeckner, E., Schlese, U., Schulzweida, U. and Tyree, M. 1994 Forecasting global ENSO-related climate anomalies. *Tellus*, **46a**, 367–380

Barnett, T. P., Arpe, K., Bengtsson, L., Ji, M. and Kumar, A. 1997 Potential predictability and AMIP implications of midlatitude climate variability in two general circulation models. *J. Climate*, **10**, 2321–2329

Bengtsson, L., Schlese, U., Roeckner, E., Latif, M., Barnett, T. P. and Graham, N. 1993 A two-tiered approach to long-range climate forecasting. *Science*, **161**, 1026–1029

Branković, Č. and Palmer, T. N. 1997 Atmospheric seasonal predictability and estimates of ensemble size. *Mon. Weather Rev.*, **125**, 859–874

Christoph, M., Barnett, T. P. and Roeckner, E. 1997 The Antarctic circumpolar wave in a coupled ocean–atmosphere GCM. *J. Climate*, **11**, 1659–1672

Dix, M. R. and Hunt, B. G. 1995 Chaotic influences and the problem of deterministic seasonal prediction. *Int. J. Climatol.*, **15**, 729–752

Fraedrich, K. and Müller, K. 1992 Climate anomalies in Europe associated with ENSO extremes. *Int. J. Climatol.*, **12**, 25–31

Frey, H., Latif, M. and Stockdale, T. 1997 The coupled GCM ECHO2. Part I: The tropical Pacific. *Mon. Weather Rev.*, **125**, 703–720

Goddard, L. and Graham, N. E. 1999 Importance of the Indian Ocean for simulating rainfall anomalies over eastern and southern Africa. *J. Geophys. Res.*, **104 D16**, 19099–19116

Halpert, M. S. and Ropolewski, C. F. 1992 Temperature patterns associated with the Southern Oscillation. *J. Climate*, **5**, 577–593

Harzallah, A. and Sadourny, R. 1995 Internal versus SST-forced atmospheric variability as simulated by an atmospheric general circulation model. *J. Climate*, **8**, 474–495

Hoerling, M. P. and Kumar, A. 1997 Origins of extreme climate states during the 1982–83 ENSO winter. *J. Climate*, **10**, 2859–2870

Hulme, M. 1991 An intercomparison of model and observed global precipitation climatologies. *Geophys. Res. Lett.*, **18**, 1715–1718

Kumar, A. and Hoerling, M. P. 1995 Prospects and limitations of seasonal atmospheric GCM predictions. *Bull. Am. Meteorol. Soc.*, **76**, 335–345

Kumar, A., Hoerling, M. P., Ji, M., Leetmaa, A. and Sardeshmukh, P. 1996 Assessing a GCM's suitability for making seasonal predictions. *J. Climate*, **9**, 115–129

Latif, M., Kleeman, R. and Eckert, C. 1997 Greenhouse warming, decadal variability, or El Niño? An attempt to understand the anomalous 1990s. *J. Climate*, **10**, 2221–2239

Latif, M., Dommenget, D., Dima, M. and Grötzner, A. 1999 The role of Indian Ocean sea surface temperature in forcing east African rainfall anomalies during December–January 1997/98. *J. Climate*, **12**, 3497–3504

Moron, V., Navarra, A., Ward, M. N. and Roeckner, E. 1998 Skill and reproducibility of seasonal rainfall patterns in the tropics in ECHAM-4 GCM simulations with prescribed SST. *Clim. Dyn.*, **14**, 83–100

Oberhuber, J. M., Roeckner, E., Christoph, M., Esch, M. and Latif, M. 1998 Predicting the '97 El Niño event with a global climate model. *Geophys. Res. Lett.*, **25**, 2273–2276

Pan, Y. H. and Oort, A. H. 1983 Global climate variations connected with sea surface temperature anomalies in the eastern equatorial Pacific Ocean for the 1958–73 period. *Mon. Weather Rev.*, **111**, 1244–1258

Palmer, T. N. and Anderson, D. L. T. 1994 The prospects of seasonal forecasting—A review paper. *Q. J. R. Meteorol. Soc.*, **120**, 755–793

Rayner, N. A., Horton, E. B., Parker, D. E., Folland, C. K. and Hackett, R. B. 1996 'Version 2.2 of the global sea-ice and sea surface temperature dataset, 1903–94'. Climate Research Technical Note 74. Available from the Hadley Centre for Climate Prediction and Research, The Met. Office, Bracknell, UK

Reynolds, R. W. and Smith, T. M. 1994 Improved global sea surface temperature analyses using optimum interpolation. *J. Climate*, **7**, 929–948

Rocha, A. and Simmonds, I. 1997 Interannual variability of south-eastern African summer rainfall. Part 1: Relationships with air–sea interaction processes. *Int. J. Climatol.*, **17**, 235–265

Roeckner, E., Arpe, K., Bengtsson, L., Christoph, M., Claussen, M., Dümenil, L., Esch, M., Giorgetta, M., Schlese, U. and Schulzweida, U. 1996a 'The atmospheric general circulation model ECHAM4: Model description and simulation of present-day climate'. Max-Planck-Institut für Meteorologie, Report No. 218, Hamburg, Germany

Roeckner, E., Oberhuber, J. M., Bacher, A., Christoph, M. and Kirchner, I. 1996b ENSO variability and atmospheric response in a global coupled atmosphere–ocean GCM. *Clim. Dyn.*, **12,** 737–754

Ropolewski, C. F. and Halpert, M. S. 1987 Global and regional scale precipitation patterns associated with the El Niño/Southern Oscillation. *Mon. Weather Rev.*, **115,** 1606–1626

Rowell, D. P. 1998 Assessing potential seasonal predictability with an ensemble of multidecadal GCM simulations. *J. Climate*, **11,** 109–120

Rowell, D. P., Folland, C. K., Maskell, K. and Ward, M. N. 1995 Variability of summer rainfall over tropical North Africa (1906–92): Observations and modelling. *Q. J. R. Meteorol. Soc.*, **121,** 669–704

Siegel, S. 1956 Pp. 116–127 in *Nonparametric statistics for the behavioral sciences*. McGraw-Hill Kogakusha, Tokyo, Japan

Smith, I. N. 1995 A GCM simulation of global climate interannual variability: 1950–1988. *J. Climate*, **8,** 709–718

Stern, W. and Miyakoda, K. 1995 The feasibility of seasonal forecasts speculated from multiple GCM simulations. *J. Climate*, **8,** 1071–1078

Stockdale, T. N., Anderson, D. L. T., Alves, J. O. S. and Balmaseda, M. A. 1998 Global seasonal rainfall forecasts using a coupled ocean–atmosphere model. *Nature*, **392,** 370–373

Trenberth, K. E., Branstator, G. W., Karoly, D., Kumar, A., Lau, N. C. and Ropolewski, C. 1998 Progress during TOGA in understanding and modeling global teleconnections associated with tropical sea surface temperatures. *J. Geophys. Res.*, **103,** 14291–14325

Venzke, S., Latif, M. and Villwock, A. 1999 The coupled GCM ECHO-2: Indian Ocean response to ENSO. *J. Climate*, **13,** 1371–1373

Wallace, J. M., Rasmusson, E. M., Mitchell, T. P., Kousky, V. E., Sarachik, E. S. and von Storch, H. 1998 On the structure and evolution of ENSO-related climate variability in the tropical Pacific: Lessons from TOGA. *J. Geophys. Res.*, **103 C7,** 14241–14259

Webster, P. J., Moore, A. M., Loschnigg, J. P. and Leben, R. R. 1999 Coupled ocean–atmosphere dynamics in the Indian Ocean during 1997–98. *Nature*, **401,** 356–360

White, W. B. and Peterson, R. G. 1996 An Antarctic circumpolar wave in surface pressure, wind, temperature and sea-ice extent. *Nature*, **280,** 699–702

Xie, P. and Arkin, P. A. 1997 Global precipitation: A 17-year monthly analysis based on gauge observations, satellite estimates and numerical model outputs. *Bull. Am. Meteorol. Soc.*, **78,** 2539–2558

Yang, X., Anderson, J. L. and Stern, W. F. 1998 Reproducible forced modes in AGCM ensemble integrations and potential predictability of atmospheric seasonal variations in the extratropics. *J. Climate*, **11,** 2942–2959

Zwiers, F. W. 1996 Interannual variability and predictability in an ensemble of AMIP climate simulations conducted with the CCC GCM2. *Clim. Dyn.*, **12,** 825–848